

Enhanced left/right asymmetry in reflection and transmission due to a periodic multilayer of a topological insulator and an anisotropic dielectric material

Francesco Chiadini

Department of Industrial Engineering, University of Salerno, via Giovanni Paolo II, 132 – Fisciano (SA), I-84084, Italy

Vincenzo Fiumara

School of Engineering, University of Basilicata, Viale dell'Ateneo Lucano 10, 85100 Potenza, Italy

Akhlesh Lakhtakia

Department of Engineering Science and Mechanics, Pennsylvania State University, University Park, PA 16802–6812, USA

Antonio Scaglione

Department of Industrial Engineering, University of Salerno, via Giovanni Paolo II, 132 – Fisciano (SA), I-84084, Italy

Abstract

Very weak left/right asymmetry in reflection and transmission is offered by a layer of a topological insulator on top of a layer of an anisotropic dielectric material, but it can be enhanced very significantly by using a periodic multilayer of both types of materials. This is an attractive prospect for realizing one-way terahertz devices, because both types of materials can be grown using standard physical-vapor-deposition techniques.

Introduction

A topological insulator (TI) [1, 2, 3] possesses topologically protected surface states leading to an electromagnetic constitution that must be characterized not only in volumetric terms but also in terms of a surface admittance [4]. Interest in TIs has greatly grown during the past decade as many materials, such as Bi_2Se_3 and Sb_2Te_3 , have been experimentally confirmed to be topological insulators [5, 6, 7]. Mixed materials and new material compositions [2, 3, 8, 9] carry promise, especially because the surface admittance can be enhanced by the application of a magnetostatic field [7, 10].

The topologically protected surface states have macroscopic consequences in optics [12, 13, 14, 11]. Optical modeling of a TI can be accomplished in two different, though equivalent, ways [4]:

- (i) as a bi-isotropic material that is nonreciprocal in the Lorentz sense [15, 16] with the nonreciprocity quantified by a magnetoelectric pseudoscalar denoted by γ_{TI} [13, 14], or
- (ii) as an isotropic dielectric material with a surface admittance denoted by γ_{TI} [4].

From a macroscopic point of view, topological insulation is a phenomenon manifesting itself at the surface but not in the bulk; hence we preferred to model TIs using the surface admittance. This choice also satisfies the Post constraint [17] that is mandated by the mathematical structure of modern electromagnetic theory.

When light is incident on an infinitely extended layer of a homogeneous material, some is reflected and some is transmitted [13, 14]. The direction of propagation of the incident light is described by two angles: (a) $\theta \in [0^\circ, 90^\circ)$ between the direction of propagation and the normal to the illuminated face of the layer, and (b) $\psi \in [0^\circ, 360^\circ)$ between the projection of the direction of propagation on the illuminated face and a straight line drawn on the face. As a TI is an isotropic dielectric material, the reflectances and transmittances of a TI layer do not depend on ψ [18]. However, if a TI were an anisotropic dielectric material, the reflectances and transmittances would exhibit asymmetry with respect to the reversal of projection of the direction of propagation of the incident plane wave on the illuminated face. In other words, if θ were kept fixed by ψ were to be replaced by $\psi + 180^\circ$, the reflectances and transmittances would change [18].

Theory shows that left/right reflection asymmetry can be exhibited by a cascade of a layer of an anisotropic dielectric material and a TI layer [19]. If strong enough, left/right reflection asymmetry could enable one-way optical devices that can reduce back-scattering noise as well as instabilities in optical communication networks; help efficiently deliver internet at ultrahigh baud rates through lighting fixtures; and

sharpen 2D and 3D images for microscopy, tomography, process control, and surgeries. But, in all studies reported thus far, the magnitude of the surface admittance required is much greater than the value that can be effectively achieved [20].

In a bid to enhance left/right reflection asymmetry, we theoretically investigated reflection and transmission characteristics of a periodic multilayer in which identical columnar thin films (CTFs) are interspersed with identical TI layers. A CTF is an ensemble of parallel nanowires aligned obliquely on a planar substrate [21, 22]. Usually grown by physical vapor deposition [24, 23, 25, 26], a CTF is a macroscopically homogeneous and orthorhombic biaxial dielectric material [27]. The optical response characteristics of CTFs have been exploited for various optical applications [22].

In this paper we report the results of our investigation in which we kept γ_{TI} at a low (feasible) value and we used data for a CTF of tantalum oxide [27, 28, 29]. The paper is organized as follows: in Sec. 1 we describe in details the materials used and the method to calculate the transmittance/reflectance. In Sec. 2 results showing the left/right asymmetry in the periodic CTF/TI multilayer are presented and discussed. Conclusions follow in Sec. 3.

An $\exp(-i\omega t)$ dependence on time t is implicit, with ω denoting the angular frequency and $i = \sqrt{-1}$. The free-space wavenumber, the free-space wavelength, and the intrinsic impedance of free space are denoted by $k_0 = \omega\sqrt{\varepsilon_0\mu_0}$, $\lambda_0 = 2\pi/k_0$, and $\eta_0 = \sqrt{\mu_0/\varepsilon_0}$, respectively, with ε_0 and μ_0 being the permeability and permittivity of free space. The speed of light in vacuum is denoted by $c_0 = 1/\sqrt{\varepsilon_0\mu_0}$, the reduced Planck constant by \hbar , and the charge of an electron by q_e . Vectors are in boldface; Cartesian unit vectors are identified as \mathbf{u}_x , \mathbf{u}_y , and \mathbf{u}_z ; $\mathbf{r} = x\mathbf{u}_x + y\mathbf{u}_y + z\mathbf{u}_z$ is the position vector; dyadics are underlined twice; column vectors are in boldface and enclosed in square brackets; and matrices are double underlined and enclosed in square brackets.

1 Theory

We suppose that the half spaces $z < 0$ and $z > L_\Sigma = N\Lambda + L_{\text{subs}}$ are occupied by air. The region $0 < z < L_\sigma = N\Lambda$ is occupied by a periodic multilayer made of N unit cells. The multilayer is of infinite extent in the xy plane. Each unit cell of thickness $\Lambda = L_{\text{TI}} + L_{\text{CTF}}$ comprises a TI of thickness L_{TI} and a CTF of thickness L_{CTF} . The relative permittivity scalar of the TI is denoted by ε_{TI} . The 3×3 relative permittivity matrix of the CTF is expressed as [21, 27, 28, 29]

$$\underline{\underline{\varepsilon}}_{\text{CTF}} = \begin{bmatrix} \varepsilon_b + (\varepsilon_a - \varepsilon_b) \sin^2 \chi & 0 & -\frac{1}{2}(\varepsilon_a - \varepsilon_b) \sin 2\chi \\ 0 & \varepsilon_c & 0 \\ -\frac{1}{2}(\varepsilon_a - \varepsilon_b) \sin 2\chi & 0 & \varepsilon_a - (\varepsilon_a - \varepsilon_b) \sin^2 \chi \end{bmatrix}, \quad (1)$$

where $\varepsilon_{a,b,c}$ are the eigenvalues of $\underline{\underline{\varepsilon}}_{\text{CTF}}$ and the angle $\chi \in (0^\circ, 90^\circ]$. The region $L_\sigma < z < L_\Sigma$ is occupied by a dielectric material functioning as a substrate, its relative permittivity scalar being denoted by $\varepsilon_{\text{subs}}$.

A plane wave is incident at an angle θ with respect to the z axis and at an angle ψ with respect to the x axis in the xy plane, as illustrated in Fig. 1. The wave vector of the incident plane wave can therefore be written as

$$\mathbf{k}_{\text{inc}} = \kappa (\mathbf{u}_x \cos \psi + \mathbf{u}_y \sin \psi) + \mathbf{u}_z k_0 \cos \theta, \quad (2)$$

where $\kappa = k_0 \sin \theta$. The electric and magnetic field phasors of the incident plane wave are given by

$$\begin{cases} \mathbf{E}_{\text{inc}}(\mathbf{r}) &= \mathbf{E}_{0,\text{inc}} \exp(i\mathbf{k}_{\text{inc}} \cdot \mathbf{r}) \\ \mathbf{H}_{\text{inc}}(\mathbf{r}) &= \mathbf{H}_{0,\text{inc}} \exp(i\mathbf{k}_{\text{inc}} \cdot \mathbf{r}) \end{cases}, \quad z < 0, \quad (3)$$

where the amplitude vectors are represented by column 3-vectors as

$$[\mathbf{E}_{0,inc}] = \begin{bmatrix} E_{x,inc} \\ E_{y,inc} \\ E_{z,inc} \end{bmatrix} = \begin{bmatrix} -\sin \psi & -\cos \psi \cos \theta \\ \cos \psi & -\sin \psi \cos \theta \\ 0 & \sin \theta \end{bmatrix} \begin{bmatrix} a_s \\ a_p \end{bmatrix} \quad (4)$$

and

$$[\mathbf{H}_{0,inc}] = \begin{bmatrix} H_{x,inc} \\ H_{y,inc} \\ H_{z,inc} \end{bmatrix} = \eta_0^{-1} \begin{bmatrix} -\cos \psi \cos \theta & \sin \psi \\ -\sin \psi \cos \theta & -\cos \psi \\ \sin \theta & 0 \end{bmatrix} \begin{bmatrix} a_s \\ a_p \end{bmatrix}. \quad (5)$$

The scalar coefficients with a_s and a_p of the s - and p -polarized components, respectively, are assumed to be known [21, 30].

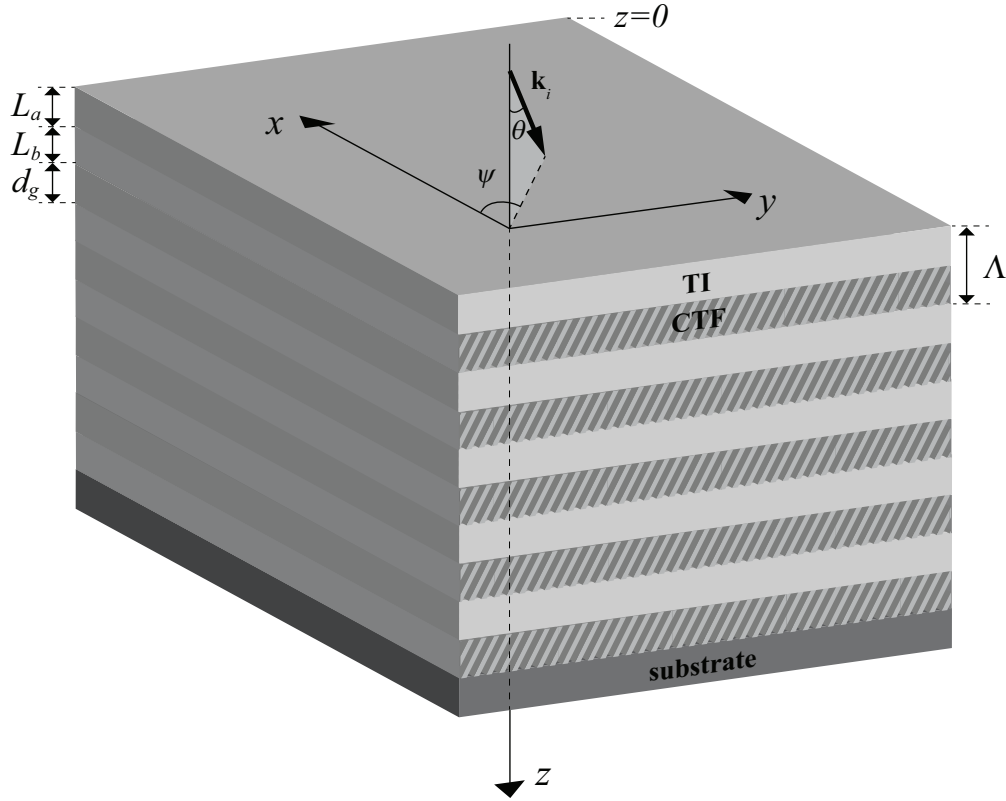


Figure 1: Schematic of the boundary-value problem solved. The structure shown has $N = 5$ unit cells and is infinitely extended in the xy plane.

The wave vector of the reflected plane wave is consequently given by

$$\mathbf{k}_{ref} = \kappa (\mathbf{u}_x \cos \psi + \mathbf{u}_y \sin \psi) - \mathbf{u}_z k_0 \cos \theta, \quad (6)$$

and the electric and magnetic field phasors as

$$\begin{cases} \mathbf{E}_{ref}(\mathbf{r}) = \mathbf{E}_{0,ref} \exp(i\mathbf{k}_{ref} \cdot \mathbf{r}) \\ \mathbf{H}_{ref}(\mathbf{r}) = \mathbf{H}_{0,ref} \exp(i\mathbf{k}_{ref} \cdot \mathbf{r}) \end{cases}, \quad z < 0, \quad (7)$$

where the amplitude vectors

$$[\mathbf{E}_{0,ref}] = \begin{bmatrix} E_{x,ref} \\ E_{y,ref} \\ E_{z,ref} \end{bmatrix} = \begin{bmatrix} -\sin \psi & \cos \psi \cos \theta \\ \cos \psi & \sin \psi \cos \theta \\ 0 & \sin \theta \end{bmatrix} \begin{bmatrix} r_s \\ r_p \end{bmatrix} \quad (8)$$

and

$$[\mathbf{H}_{0,ref}] = \begin{bmatrix} H_{x,ref} \\ H_{y,ref} \\ H_{z,ref} \end{bmatrix} = \eta_0^{-1} \begin{bmatrix} \cos \psi \cos \theta & \sin \psi \\ \sin \psi \cos \theta & -\cos \psi \\ \sin \theta & 0 \end{bmatrix} \begin{bmatrix} r_s \\ r_p \end{bmatrix} \quad (9)$$

employ r_s and r_p as the unknown coefficients of the s - and p -polarized components, respectively [21, 30].

The wave vector of the transmitted plane wave is exactly the same as that of the incident plane wave. Therefore, the electric and magnetic field phasors of the transmitted plane wave are

$$\begin{cases} \mathbf{E}_{trs}(\mathbf{r}) = \mathbf{E}_{0,trs} \exp[i\mathbf{k}_{inc} \cdot (\mathbf{r} - L_\Sigma \mathbf{u}_z)] \\ \mathbf{H}_{trs}(\mathbf{r}) = \mathbf{H}_{0,trs} \exp[i\mathbf{k}_{inc} \cdot (\mathbf{r} - L_\Sigma \mathbf{u}_z)] \end{cases}, \quad z > L_\Sigma, \quad (10)$$

where the column 3-vectors

$$[\mathbf{E}_{0,trs}] = \begin{bmatrix} E_{x,trs} \\ E_{y,trs} \\ E_{z,trs} \end{bmatrix} = \begin{bmatrix} -\sin \psi & -\cos \psi \cos \theta \\ \cos \psi & -\sin \psi \cos \theta \\ 0 & \sin \theta \end{bmatrix} \begin{bmatrix} t_s \\ t_p \end{bmatrix} \quad (11)$$

and

$$[\mathbf{H}_{0,trs}] = \begin{bmatrix} H_{x,trs} \\ H_{y,trs} \\ H_{z,trs} \end{bmatrix} = \eta_0^{-1} \begin{bmatrix} -\cos \psi \cos \theta & \sin \psi \\ -\sin \psi \cos \theta & -\cos \psi \\ \sin \theta & 0 \end{bmatrix} \begin{bmatrix} t_s \\ t_p \end{bmatrix} \quad (12)$$

contain t_s and t_p as the unknown coefficients of the s - and p -polarized components, respectively [21, 30]. A boundary-value problem has to be solved in order to determine the coefficients r_s , r_p , t_s , and t_p in terms of a_s and a_p .

The electric and magnetic field phasors everywhere are conveniently represented as [21]

$$\begin{cases} \mathbf{E}(\mathbf{r}) = \mathbf{e}(z) \exp[i\kappa(x \cos \psi + y \sin \psi)] \\ \mathbf{H}(\mathbf{r}) = \mathbf{h}(z) \exp[i\kappa(x \cos \psi + y \sin \psi)] \end{cases}. \quad (13)$$

Furthermore, we define the column 4-vector

$$[\mathbf{f}(z)] = \begin{bmatrix} \mathbf{u}_x \cdot \mathbf{e}(z) \\ \mathbf{u}_y \cdot \mathbf{e}(z) \\ \mathbf{u}_x \cdot \mathbf{h}(z) \\ \mathbf{u}_y \cdot \mathbf{h}(z) \end{bmatrix}. \quad (14)$$

Together, eq. (4), eq. (5), eq. (8), and eq. (9) yield

$$[\mathbf{f}(0^-)] = [\underline{K}] \begin{bmatrix} a_s \\ a_p \\ r_s \\ r_p \end{bmatrix}, \quad (15)$$

where the 4×4 matrix

$$[\underline{K}] = \begin{bmatrix} -\sin \psi & \cos \psi \cos \theta & -\sin \psi & \cos \psi \cos \theta \\ -\cos \psi & -\sin \psi \cos \theta & \cos \psi & \sin \psi \cos \theta \\ -\eta_0^{-1} \cos \psi \cos \theta & \eta_0^{-1} \sin \psi & \eta_0^{-1} \cos \psi \cos \theta & \eta_0^{-1} \sin \psi \\ -\eta_0^{-1} \sin \psi \cos \theta & \eta_0^{-1} \cos \psi & \eta_0^{-1} \sin \psi \cos \theta & -\eta_0^{-1} \cos \psi \end{bmatrix}. \quad (16)$$

Together, eq. (11) and eq. (12) yield

$$[\mathbf{f}(L_{\Sigma}^+)] = [\underline{K}] \begin{bmatrix} t_s \\ t_p \\ 0 \\ 0 \end{bmatrix} \quad (17)$$

The n th unit cell, $n \in [1, N]$, occupies the region $z_{n-1} < z < z_n$, where $z_n = n\Lambda$. The region $z_{n-1} < z < \zeta_n = z_{n-1} + L_{\text{TI}}$ is occupied by the chosen TI. In this region, $[\mathbf{f}(z)]$ obeys the 4×4 matrix ordinary differential equation

$$\frac{d}{dz} [\mathbf{f}(z)] = i [\underline{P}]_{\text{TI}} [\mathbf{f}(z)], \quad z_{n-1} < z < \zeta_n, \quad (18)$$

where the 4×4 matrix

$$\begin{aligned} [\underline{P}]_{\text{TI}} = & \omega \begin{bmatrix} 0 & 0 & 0 & \mu_0 \\ 0 & 0 & -\mu_0 & 0 \\ 0 & -\varepsilon_0 \varepsilon_{\text{TI}} & 0 & 0 \\ \varepsilon_0 \varepsilon_{\text{TI}} & 0 & 0 & 0 \end{bmatrix} \\ & + \frac{\kappa^2}{\omega \varepsilon_0 \varepsilon_{\text{TI}}} \begin{bmatrix} 0 & 0 & \cos \psi \sin \psi & -\cos^2 \psi \\ 0 & 0 & \sin^2 \psi & -\cos \psi \sin \psi \\ 0 & 0 & 0 & 0 \\ 0 & 0 & 0 & 0 \end{bmatrix} \\ & + \frac{\kappa^2}{\omega \mu_0} \begin{bmatrix} 0 & 0 & 0 & 0 \\ 0 & 0 & 0 & 0 \\ -\cos \psi \sin \psi & \cos^2 \psi & 0 & 0 \\ -\sin^2 \psi & \cos \psi \sin \psi & 0 & 0 \end{bmatrix}. \end{aligned} \quad (19)$$

The solution of eq. (18) delivers [31]

$$[\mathbf{f}(\zeta_n^-)] = [\underline{Q}]_{\text{TI}} [\mathbf{f}(z_{n-1}^+)], \quad (20)$$

where the 4×4 matrix

$$[\underline{Q}]_{\text{TI}} = \exp \left\{ i [\underline{P}]_{\text{TI}} L_{\text{TI}} \right\}. \quad (21)$$

The region $\zeta_n < z < z_n$ is occupied by the chosen CTF. In this region, $[\mathbf{f}(z)]$ obeys the 4×4 matrix ordinary differential equation [21]

$$\frac{d}{dz} [\mathbf{f}(z)] = i [\underline{P}]_{\text{CTF}} [\mathbf{f}(z)], \quad \zeta_n < z < z_n, \quad (22)$$

where the 4×4 matrix

$$\begin{aligned}
\underline{\underline{P}}_{CTF} &= \omega \begin{bmatrix} 0 & 0 & 0 & \mu_0 \\ 0 & 0 & -\mu_0 & 0 \\ 0 & -\varepsilon_0 \varepsilon_c & 0 & 0 \\ \varepsilon_0 \varepsilon_d & 0 & 0 & 0 \end{bmatrix} \\
&+ \kappa \frac{\varepsilon_d (\varepsilon_a - \varepsilon_b) \sin 2\chi}{\varepsilon_a \varepsilon_b} \begin{bmatrix} \cos \psi & 0 & 0 & 0 \\ \sin \psi & 0 & 0 & 0 \\ 0 & 0 & 0 & 0 \\ 0 & 0 & -\sin \psi & \cos \psi \end{bmatrix} \\
&+ \frac{\kappa^2}{\omega \varepsilon_0} \frac{\varepsilon_d}{\varepsilon_a \varepsilon_b} \begin{bmatrix} 0 & 0 & \cos \psi \sin \psi & -\cos^2 \psi \\ 0 & 0 & \sin^2 \psi & -\cos \psi \sin \psi \\ 0 & 0 & 0 & 0 \\ 0 & 0 & 0 & 0 \end{bmatrix} \\
&+ \frac{\kappa^2}{\omega \mu_0} \begin{bmatrix} 0 & 0 & 0 & 0 \\ 0 & 0 & 0 & 0 \\ -\cos \psi \sin \psi & \cos^2 \psi & 0 & 0 \\ -\sin^2 \psi & \cos \psi \sin \psi & 0 & 0 \end{bmatrix} \tag{23}
\end{aligned}$$

employs

$$\varepsilon_d = \frac{\varepsilon_a \varepsilon_b}{\varepsilon_a \cos^2 \chi + \varepsilon_b \sin^2 \chi} . \tag{24}$$

The solution of eq. (22) delivers [31]

$$[\mathbf{f}(z_n^-)] = \underline{\underline{Q}}_{CTF} [\mathbf{f}(\zeta_n^+)] , \tag{25}$$

where the 4×4 matrix

$$\underline{\underline{Q}}_{CTF} = \exp \left\{ i \underline{\underline{P}}_{CTF} L_{CTF} \right\} . \tag{26}$$

As shown elsewhere [19], consideration of the boundary conditions at the the interface $z = \zeta_n$ of the TI layer and the CTF yields

$$[\mathbf{f}(\zeta_n^+)] = \underline{\underline{V}} [\mathbf{f}(\zeta_n^-)] \tag{27}$$

where the 4×4 matrix

$$\underline{\underline{V}} = \begin{bmatrix} 1 & 0 & 0 & 0 \\ 0 & 1 & 0 & 0 \\ -\gamma_{TI} & 0 & 1 & 0 \\ 0 & -\gamma_{TI} & 0 & 1 \end{bmatrix} . \tag{28}$$

Accordingly,

$$[\mathbf{f}(z_n^-)] = \underline{\underline{Q}}_{CTF} \underline{\underline{V}} \underline{\underline{Q}}_{TI} [\mathbf{f}(z_{n-1}^+)] . \tag{29}$$

Consideration of the boundary conditions at the interface $z = z_{n-1}$ yields [19]

$$[\mathbf{f}(z_{n-1}^+)] = \underline{\underline{V}}^{-1} [\mathbf{f}(z_{n-1}^-)] . \tag{30}$$

From the last two equations, we obtain

$$\left[\mathbf{f}(z_n^-) \right] = \left[\underline{U} \right] \left[\mathbf{f}(z_{n-1}^-) \right], \quad (31)$$

where the 4×4 matrix

$$\left[\underline{U} \right] = \left[\underline{Q} \right]_{CTF} \left[\underline{V} \right] \left[\underline{Q} \right]_{TI} \left[\underline{V} \right]^{-1} \quad (32)$$

is the characteristic matrix of a unit cell. Application of eq. (31) repeatedly from $n = 1$ to $n = N$ delivers

$$\left[\mathbf{f}(L_\sigma^-) \right] = \left[\underline{U} \right]^N \left[\mathbf{f}(0^-) \right]. \quad (33)$$

The region $L_\sigma < z < L_\Sigma$ is occupied by the substrate. In this region, $[\mathbf{f}(z)]$ obeys the 4×4 matrix ordinary differential equation

$$\frac{d}{dz} \left[\mathbf{f}(z) \right] = i \left[\underline{P} \right]_{subs} \left[\mathbf{f}(z) \right], \quad L_\sigma < z < L_\Sigma, \quad (34)$$

where the 4×4 matrix $\left[\underline{P} \right]_{subs}$ is obtained by replacing ε_{TI} by ε_{subs} on the right side of eq. (19). The solution of eq. (34) delivers [31]

$$\left[\mathbf{f}(L_\Sigma^-) \right] = \left[\underline{Q} \right]_{subs} \left[\mathbf{f}(L_\sigma^+) \right], \quad (35)$$

where the 4×4 matrix

$$\left[\underline{Q} \right]_{subs} = \exp \left\{ i \left[\underline{P} \right]_{subs} L_{subs} \right\}. \quad (36)$$

Application of the standard boundary conditions [30] at the interface $z = L_\sigma$ yields

$$\left[\mathbf{f}(L_\sigma^+) \right] = \left[\mathbf{f}(L_\sigma^-) \right], \quad (37)$$

so that

$$\left[\mathbf{f}(L_\Sigma^-) \right] = \left[\underline{Q} \right]_{subs} \left[\underline{U} \right]^N \left[\mathbf{f}(0^-) \right] \quad (38)$$

follows from eq. (33) and eq. (35). Finally, application of the standard boundary conditions [30] at the interface $z = L_\sigma$ yields

$$\left[\mathbf{f}(L_\Sigma^+) \right] = \left[\mathbf{f}(L_\Sigma^-) \right], \quad (39)$$

leading to

$$\left[\mathbf{f}(L_\Sigma^+) \right] = \left[\underline{Q} \right]_{subs} \left[\underline{U} \right]^N \left[\mathbf{f}(0^-) \right]. \quad (40)$$

Combining eq. (15), eq. (17), and eq. (40), we get

$$\begin{bmatrix} t_s \\ t_p \\ 0 \\ 0 \end{bmatrix} = \left[\underline{M} \right] \begin{bmatrix} a_s \\ a_p \\ r_s \\ r_p \end{bmatrix}, \quad (41)$$

where the 4×4 matrix

$$\left[\underline{M} \right] = \left[\underline{K} \right]^{-1} \left[\underline{Q} \right]_{subs} \left[\underline{U} \right]^N \left[\underline{K} \right] \quad (42)$$

can be partitioned into 4 2×2 submatrices as follows:

$$\left[\underline{M} \right] = \left[\begin{array}{c|c} \left[\underline{M}_{11} \right] & \left[\underline{M}_{12} \right] \\ \hline \left[\underline{M}_{21} \right] & \left[\underline{M}_{22} \right] \end{array} \right]. \quad (43)$$

Then the scalar coefficients of the reflected plane wave emerge

$$\begin{bmatrix} r_s \\ r_p \end{bmatrix} = - \left[\underline{\underline{M}}_{22} \right]^{-1} \left[\underline{\underline{M}}_{21} \right] \begin{bmatrix} a_s \\ a_p \end{bmatrix} \quad (44)$$

and the scalar coefficients of the transmitted plane wave can be calculated as

$$\begin{bmatrix} t_s \\ t_p \end{bmatrix} = \left[\underline{\underline{M}}_{tot} \right] \begin{bmatrix} a_s \\ a_p \end{bmatrix} \quad (45)$$

where

$$\left[\underline{\underline{M}}_{tot} \right] = \left[\underline{\underline{M}}_{11} \right] - \left[\underline{\underline{M}}_{12} \right] \left[\underline{\underline{M}}_{22} \right]^{-1} \left[\underline{\underline{M}}_{21} \right] \quad (46)$$

is the whole transfer matrix.

Four reflection coefficients r_{ab} and four transmission coefficients t_{ab} , $a \in \{p, s\}$ and $b \in \{p, s\}$, appear in the following relations:

$$\left. \begin{aligned} r_s &= r_{ss} a_s + r_{sp} a_p, & t_s &= t_{ss} a_s + t_{sp} a_p \\ r_p &= r_{ps} a_s + r_{pp} a_p, & t_p &= t_{ps} a_s + t_{pp} a_p \end{aligned} \right\}. \quad (47)$$

Accordingly, four reflectances are defined as $R_{sp} = |r_{sp}|^2$, etc., and four transmittances as $T_{sp} = |t_{sp}|^2$, etc. The principle of conservation of energy requires that

$$\left. \begin{aligned} 0 &\leq R_{ss} + R_{ps} + T_{ss} + T_{ps} \leq 1 \\ 0 &\leq R_{pp} + R_{sp} + T_{pp} + T_{sp} \leq 1 \end{aligned} \right\}. \quad (48)$$

The differences $1 - (R_{ss} + R_{ps} + T_{ss} + T_{ps})$ and $1 - (R_{pp} + R_{sp} + T_{pp} + T_{sp})$ indicate the fraction of the incident energy that is absorbed in the region $0 < z < L_\Sigma$.

In order to quantitate left/right reflection asymmetry, we define the functions

$$\Delta R_{ab}(\theta, \psi) = R_{ab}(\theta, \psi) - R_{ab}(\theta, \psi + 180^\circ), \quad a \in \{s, p\}, \quad b \in \{s, p\}. \quad (49)$$

Likewise, we define the functions

$$\Delta T_{ab}(\theta, \psi) = T_{ab}(\theta, \psi) - T_{ab}(\theta, \psi + 180^\circ), \quad a \in \{s, p\}, \quad b \in \{s, p\}, \quad (50)$$

in order to quantitate left/right transmission asymmetry.

2 Numerical Results

Intrinsic TIs are characterized by $\gamma_{\text{TI}} = \pm\alpha/\eta_0$, where $\alpha = (q_e^2/\hbar c_0)/4\pi\epsilon_0$ is the (dimensionless) fine structure constant [1, 2, 10, 11]. Either immersion in a magnetostatic field or a very thin coating of a magnetic material can be used to realize $\gamma_{\text{TI}} = (2m+1)\alpha/\eta_0$, $m \in \{0, \pm 1, \pm 2, \pm 3, \dots\}$. Thus, the normalized surface admittance $\bar{\gamma} = \gamma_{\text{TI}}\eta_0/\alpha$ can be either a negative or a positive integer. Whereas intrinsic TIs have $\bar{\gamma} = \pm 1$, exploitation of a magnetic field or material may increase $|\bar{\gamma}|$ realistically to 2 or 3 [10]. We fixed $\bar{\gamma} = 1$, $\epsilon_{\text{TI}} = 3$, and $L_{\text{TI}} = 649.5$ nm for all results reported here.

TIs have bandgaps not exceeding 300 meV; hence, we fixed our attention to $\lambda_0 \in [4, 5]$ μm for calculations. We chose the substrate material to be silicon with relative permittivity $\epsilon_{\text{subs}} = 11.68$ and thickness $L_{\text{subs}} = 5$ μm . Furthermore, we set $\chi = 48.50^\circ$, $\epsilon_a = 2.2532$, $\epsilon_b = 2.7737$, and $\epsilon_c = 2.5475$, based on data reported for columnar thin films of tantalum oxide [21, Sec. 7.3.3]. We also fixed $L_{\text{CTF}} = 749.5$ nm. Thus, $L_{\text{TI}} = \lambda_0/4\sqrt{\epsilon_{\text{TI}}}$ and $L_{\text{CTF}} = \lambda_0/4\sqrt{\epsilon_a}$ when $\lambda_0 = 4.5$ μm .

With $N = 1$, the maximum values of ΔR_{ab} and ΔT_{ab} , $a \in \{s, p\}$ and $b \in \{s, p\}$, did not exceed 10^{-2} for any combination of θ and ϕ . Although present, such degrees of left/right asymmetries are not unlikely to be technologically exploitable.

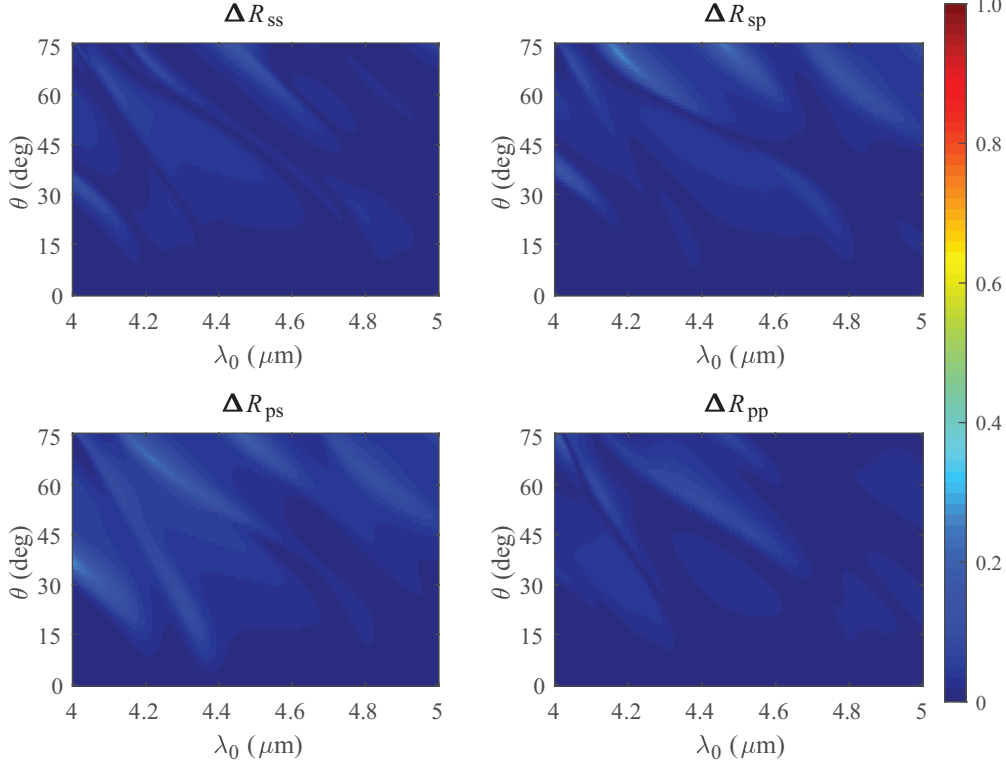


Figure 2: Left/right reflection asymmetry functions ΔR_{ss} , ΔR_{sp} , ΔR_{pp} , and ΔR_{ps} for $\theta \in [0^\circ, 90^\circ)$ and $\lambda_0 \in [4, 5]$ μm , when $\psi = 45^\circ$ and $N = 10$.

When the number of unit cells was increased from 1 to 10, left/right asymmetry appeared for both reflection and transmission. Figures 2 and 3 present density plots of all eight left/right asymmetry functions ΔR_{ab} and ΔT_{ab} , $a \in \{s, p\}$ and $b \in \{s, p\}$, for $\theta \in [0^\circ, 90^\circ)$ and $\lambda_0 \in [4, 5]$ μm , when $\psi = 45^\circ$ and $N = 10$. The asymmetry is definitely stronger in transmission than in reflection.

Further increase in the number of unit cells N intensified the left/right asymmetry in both reflection and transmission, as can be gleaned from Figs. 4 and 5 for $N = 20$, and Figs. 6 and 7 for $N = 30$. Clearly, higher values of the asymmetry functions are obtained with larger values of N and the ranges of θ and λ_0 are also enhanced thereby. Additionally, we concluded that:

- Left/right asymmetry is stronger for the transmittances than for the reflectances.
- Left/right asymmetry can be observed for quite wide ranges of the incidence angle θ and the free-space wavelength λ_0 .
- More left/right asymmetry can be achieved when the angle of incidence is $\theta \gtrsim 20^\circ$ while it vanishes, as expected, when θ approaches 0° .

For additional insights into the density plots of Figs. 2–7, the maximum values of all eight left/right asymmetry functions were identified along with the free-space wavelength $\lambda_0 \in [4, 5]$ μm and the incidence angle $\theta \in [0^\circ, 90^\circ)$ at which they occur. These data are reported in Tables 1 and 2 for reflection and transmission, respectively.

The first rows of both Tables 1, and 2 confirm that left/right asymmetry in reflection as well as transmission exists for $N = 1$, but is extremely weak. Our multilayering strategy, however, is successful in that maximum values of all eight left/right asymmetry functions increase as the number of unit cells—which is the

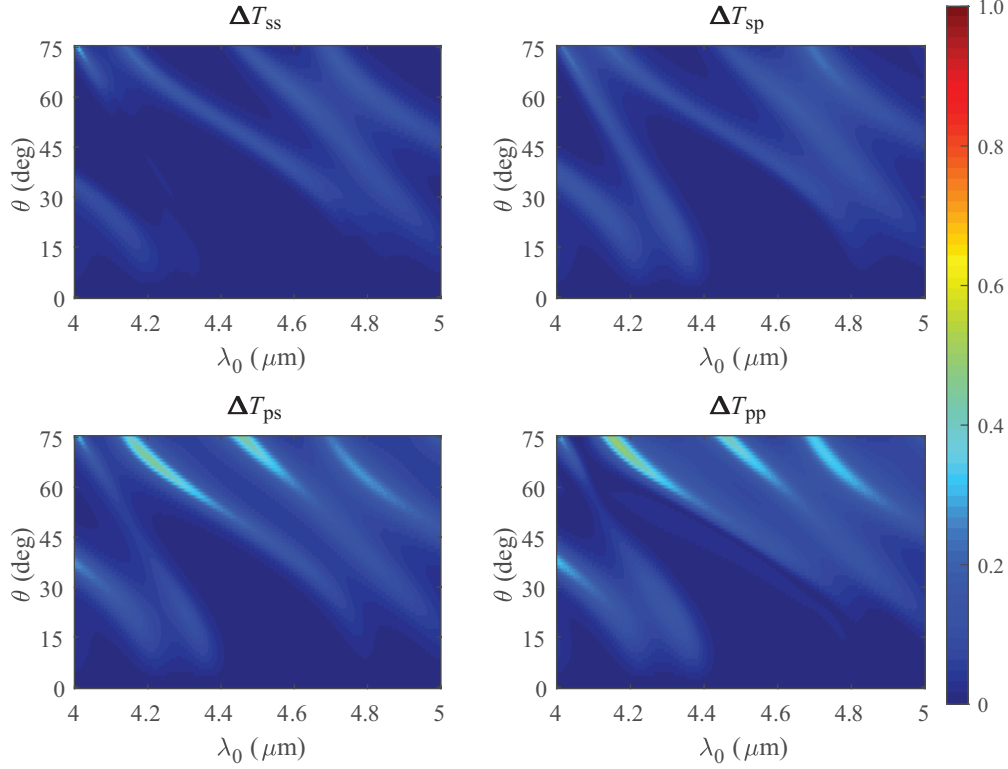


Figure 3: Left/right transmission asymmetry functions ΔT_{ss} , ΔT_{sp} , ΔT_{pp} , and ΔT_{ps} for $\theta \in [0^\circ, 90^\circ)$ and $\lambda_0 \in [4, 5]$ μm , when $\psi = 45^\circ$ and $N = 10$.

Table 1: **Maximum values of the left/right reflection asymmetry functions ΔR_{ab} , $a \in \{s, p\}$ and $b \in \{s, p\}$, along with the free-space wavelength λ_0 and the incidence angle θ at which they occur, when $\psi = 45^\circ$.**

number of cells	ΔR_{ss}			ΔR_{ps}			ΔR_{sp}			ΔR_{pp}		
	max.	$\lambda_0(\mu\text{m})$	$\theta(\text{deg})$									
$N = 1$	0.003	4.13	75	0.009	4.09	75	0.002	4.64	75	0.001	4.63	75
$N = 10$	0.145	4.43	75	0.269	4.00	36	0.256	4.18	71	0.170	4.01	75
$N = 20$	0.294	4.05	37	0.445	4.29	64	0.372	4.99	68	0.278	4.36	49
$N = 30$	0.463	4.01	41	0.449	4.99	65	0.437	4.00	41	0.380	4.01	41

Table 2: **Maximum values of the left/right transmission asymmetry functions ΔT_{ab} , $a \in \{s, p\}$ and $b \in \{s, p\}$, along with the free-space wavelength λ_0 and the incidence angle θ at which they occur, when $\psi = 45^\circ$.**

number of cells	ΔT_{ss}			ΔT_{ps}			ΔT_{sp}			ΔT_{pp}		
	max.	$\lambda_0(\mu\text{m})$	$\theta(\text{deg})$									
$N = 1$	0.005	4.09	75	0.006	4.08	75	0.005	4.08	75	0.006	4.08	75
$N = 10$	0.340	4.01	75	0.454	4.20	68	0.235	4.03	72	0.497	4.17	72
$N = 20$	0.414	4.66	51	0.617	4.32	62	0.491	4.23	25	0.654	4.27	66
$N = 30$	0.629	4.27	22	0.654	4.24	26	0.796	4.31	22	0.752	4.29	25

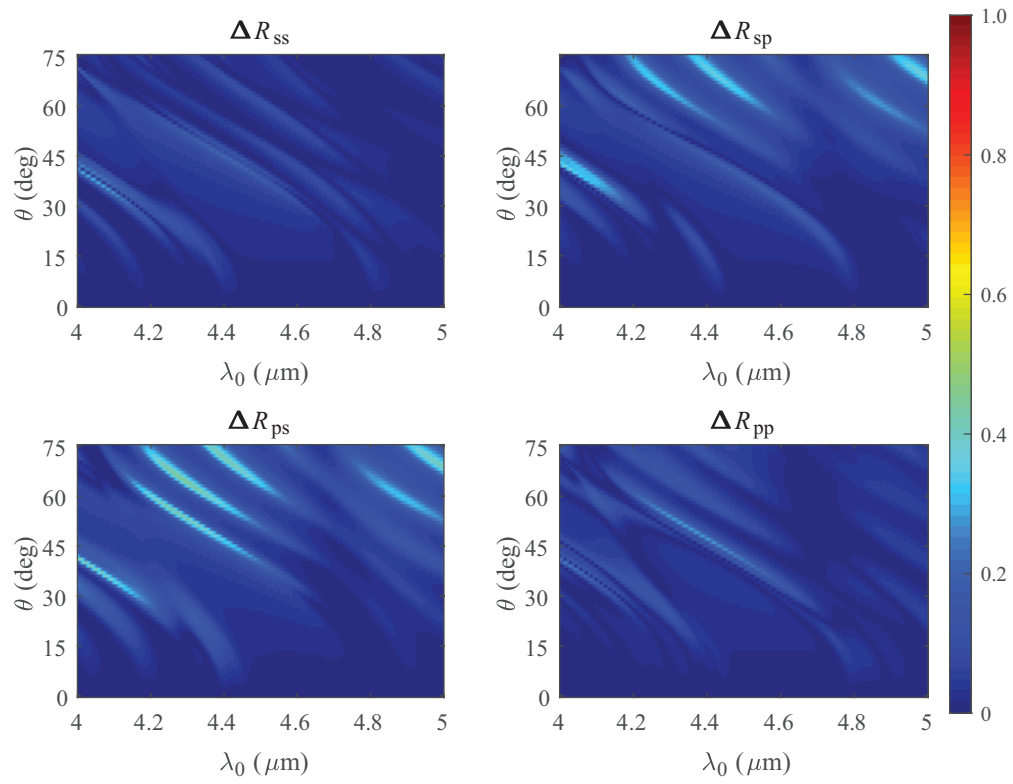


Figure 4: Same as Fig. 2 but for $N = 20$.

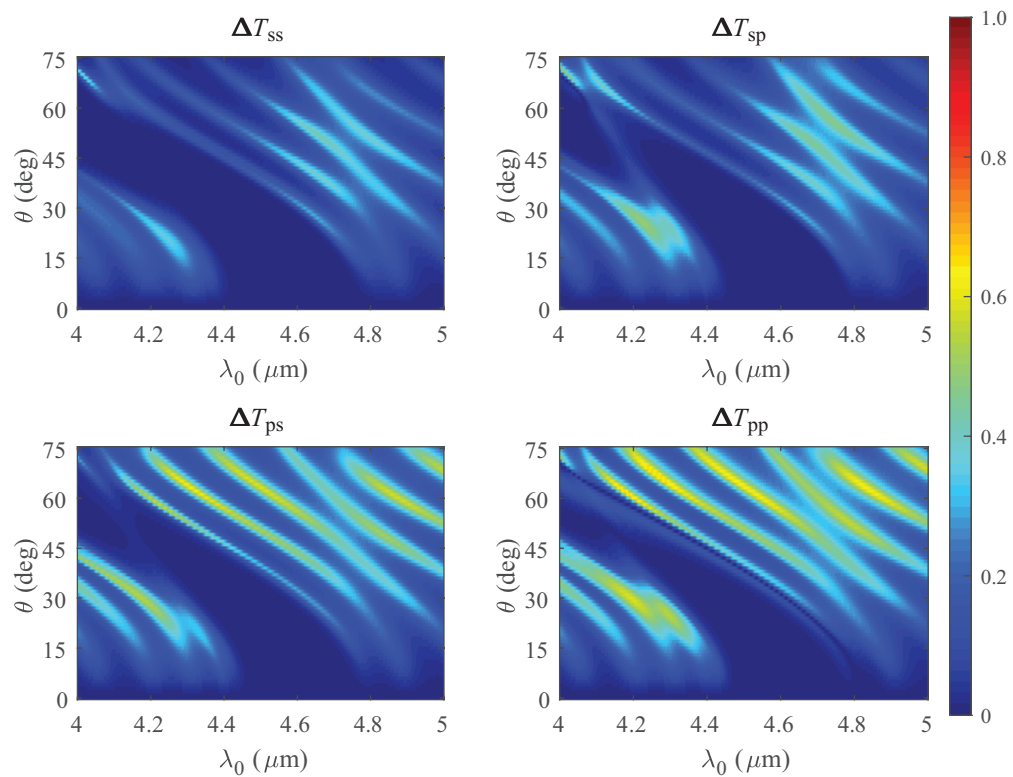


Figure 5: Same as Fig. 3 but for $N = 20$.

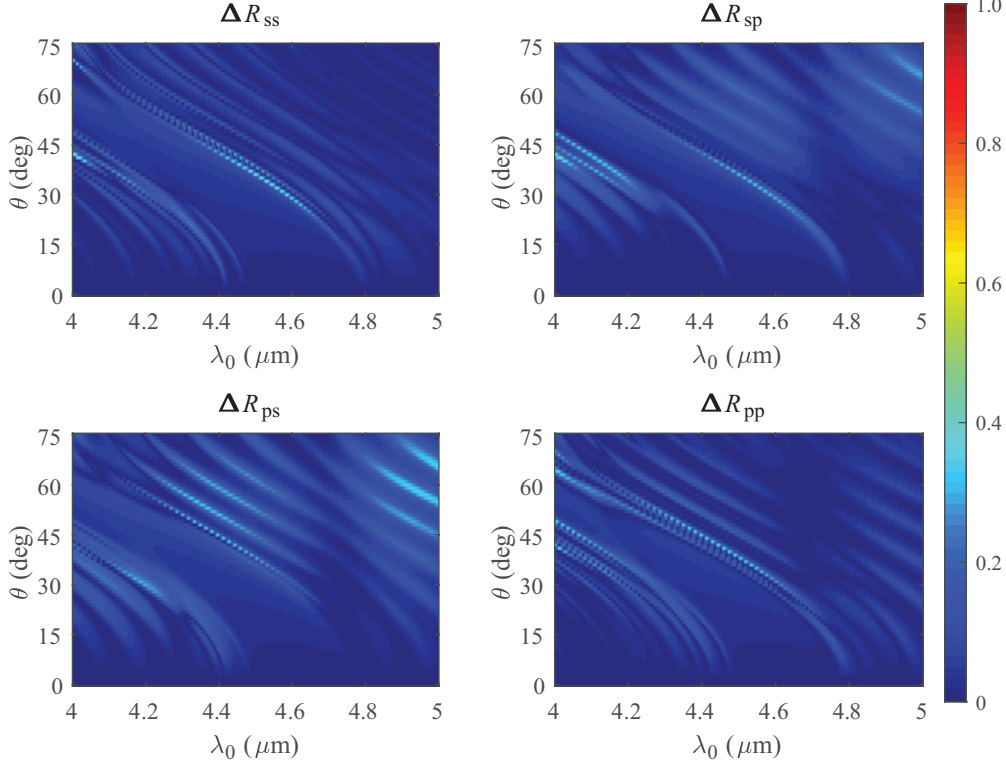


Figure 6: Same as Fig. 2 but for $N = 30$.

same as the number of TI layers—increases. However, none of the eight asymmetry functions can increase indefinitely and substantially with increasing N , because they are bounded as follows:

$$\left. \begin{array}{l} 0 \leq \Delta R_{ab} \leq 1 \\ 0 \leq \Delta T_{ab} \leq 1 \end{array} \right\}, \quad a \in \{s, p\}, \quad b \in \{s, p\}. \quad (51)$$

In other words, there will be diminishing returns for N exceeding some \bar{N} for any specific value of $\bar{\gamma}$.

3 Concluding Remarks

In an attempt to achieve a high left/right asymmetry using a topological insulator with a feasible value of the surface admittance γ_{TI} to quantitate protected surface states, we proposed and investigated a periodic-multilayer structure made of a topological insulator alternating with an anisotropic material with columnar morphology.

Analysis was performed by varying both the free-space wavelength and the direction of incidence, Left/right asymmetry is definitely evinced in both reflection and transmission by a single TI layer partnered with a layer of an anisotropic dielectric material, but the asymmetry is so weak as to be technologically unattractive. Given that TIs with larger values of γ_{TI} are presently unavailable and that the magnetic routes can probably just double or treble the magnitude of the surface admittance, the multilayering strategy proposed here offers a way to enhance left/right asymmetry in a major way, both in reflection and transmission. There will be, for sure, some maximum number of unit cells in the periodic multilayer beyond which increases in left/right asymmetry will greatly diminish, because the asymmetry functions are bounded. Still, high degrees of left/right asymmetry are going to be available, because both TI layers [9] and dense columnar thin films [22] can be deposited using standard physical-vapor-deposition techniques [24, 23, 25, 26].

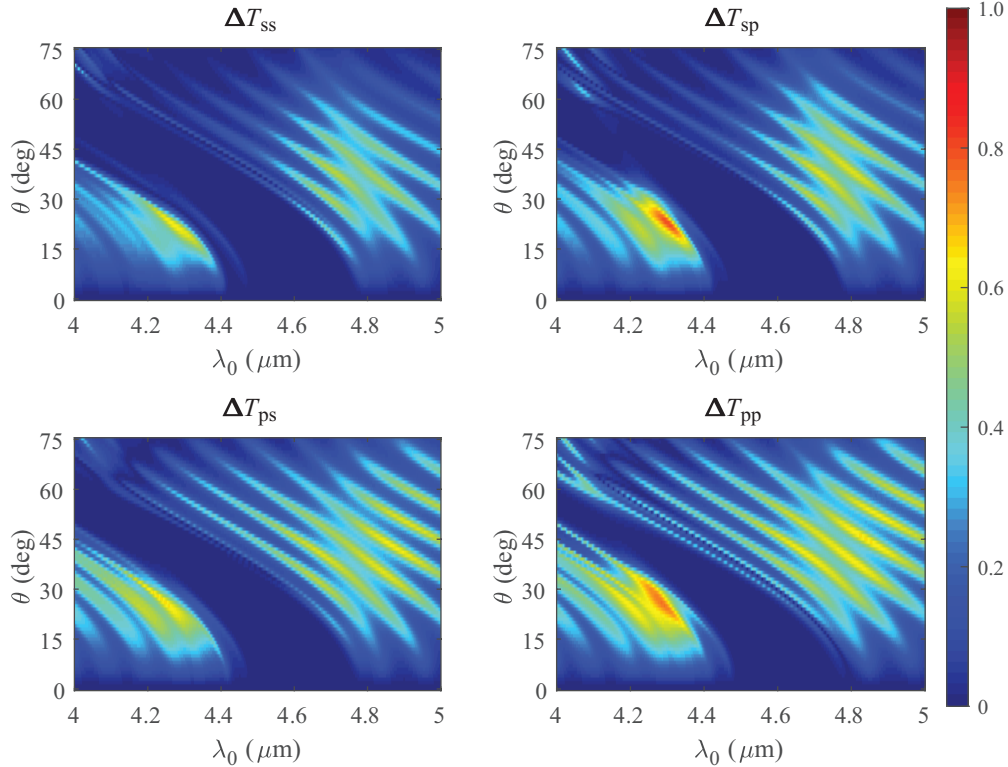


Figure 7: Same as Fig. 3 but for $N = 30$.

Acknowledgment. AL thanks the Charles Godfrey Binder Endowment at Penn State for ongoing support of his research.

References

- [1] M. Z. Hasan and C. L. Kane, “Topological insulators,” *Rev. Modern Phys.* **82**, 3045–3067 (2010).
- [2] B. Yan and S. C. Zhang, “Topological materials,” *Rep. Prog. Phys.* **75**, 096501 (2012).
- [3] Y. Ando and L. Fu, “Topological crystalline insulators and topological superconductors: From concepts to materials,” *Annu. Rev. Condens. Matter Phys.* **6**, 361–381 (2015).
- [4] A. Lakhtakia and T. G. Mackay, “Classical electromagnetic model of surface states in topological insulators,” *J. Nanophoton* **10**, 033004 (2016).
- [5] M. König, S. Wiedmann, C. Brüne, A. Roth, H. Buhmann, L. W. Molenkamp, X. L. Qi, and S.-C. Zhang, “Quantum spin Hall insulator state in HgTe quantum wells,” *Science* **318**, 766–770 (2007).
- [6] A. D. LaForge, A. Frenzel, B. C. Pursley, T. Lin, X. Liu, J. Shi, and D. N. Basov, “Optical characterization of Bi₂Se₃ in a magnetic field: Infrared evidence for magnetoelectric coupling in a topological insulator material,” *Phys. Rev. B* **81**, 125120 (2010).
- [7] C.-Z. Chang, J. Zhang, X. Feng, J. Shen, Z. Zhang, M. Guo, K. Li, Y. Ou, P. Wei, L.-L. Wang, Z.Q. Ji, Y. Feng, S. Ji S, X. Chen X, J. Jia J, J. Dai, Z. Fang, S.C. Zhang, K. He, Y. Wang Y, L. Lu, X.-C. Ma, and Q.-K. Xue, “Experimental observation of the quantum anomalous Hall effect in a magnetic topological insulator,” *Science* **340**, 167–170 (2013).

- [8] M. Barkeshli and X.L. Qi, “Topological response theory of doped topological insulators,” *Phys. Rev. Lett.* **107**, 206602 (2011).
- [9] P. Di Pietro, *Optical Properties of Bismuth-Based Topological Insulators* (Springer, 2014).
- [10] J. Maciejko, X.L. Qi, H. D. Drew, and S.C. Zhang, “Topological quantization in units of the fine structure constant,” *Phys. Rev. Lett.* **105**, 166803 (2010).
- [11] X.-L. Qi, T. L. Hughes, and S.C. Zhang, “Topological field theory of time-reversal invariant insulators,” *Phys. Rev. B* **78**, 195424 (2008).
- [12] M.-C. Chang and M.F. Yang, “Optical signature of topological insulators,” *Phys. Rev. B* **80**, 113304 (2009).
- [13] F. Liu, J. Xu, G. Song, Y. Yang, “Goos–Hänchen and Imbert–Fedorov shifts at the interface of ordinary dielectric and topological insulator,” *J. Opt. Soc. Am. B* **30**, 1167–1172 (2013).
- [14] F. Liu, J. Xu, and Y. Yang, “Polarization conversion of reflected electromagnetic wave from topological insulator,” *J. Opt. Soc. Am. B* **31**, 735–741 (2014).
- [15] H. A. Lorentz, Het theorema van Poynting over de energie in het electromagnetisch veld en een paar algemeene stellingen over de voortplanting van liet licht, *Versl. K. Akad. W. Amsterdam* **4**, 176–187 (1896).
- [16] C. M. Krowne, “Electromagnetic theorems for complex anisotropic media,” *IEEE Trans. Antennas Propagat.* **32**, 1224–1230 (1984).
- [17] E. J. Post, *Formal Structure of Electromagnetics* (North-Holland, 1962).
- [18] A. Lakhtakia and T. G. Mackay, “Left/right asymmetry in reflection and transmission by a planar anisotropic dielectric slab with topologically insulating surface states,” *J. Nanophoton.* **10**, 020501 (2016).
- [19] A. Diovisalvi, A. Lakhtakia, V. Fiumara, and F. Chiadini, “Bilaterally asymmetric reflection and transmission of light by a grating structure containing a topological insulator,” *Opt. Commun.* **398**, 67–76 (2017).
- [20] A. Lakhtakia, T. G. Mackay, F. Chiadini, A. Diovisalvi, V. Fiumara, and A. Scaglione, “How much topological insulation does one need? How much can one get?”, 2017 International Conference on Electromagnetics in Advanced Applications (ICEAA), Verona, 2017; 729–732.
- [21] A. Lakhtakia and R. Messier, *Sculptured Thin Films: Nanoengineered Morphology and Optics* (SPIE, 2005).
- [22] I. J. Hodgkinson and Q. h. Wu, *Birefringent Thin Films and Polarizing Elements* (World Scientific, 1997).
- [23] H. A. Macleod, *Thin-Film Optical Filters* (Institute of Physics, 2001).
- [24] D. M. Mattox, *The Foundations of Vacuum Coating Technology* (Noyes Publication, 2003).
- [25] R. J. Martín-Palma and A. Lakhtakia, *Nanotechnology: A Crash Course* (SPIE, 2010).
- [26] P. W. Baumeister, *Optical Coating Technology* (SPIE, 2004).
- [27] I. J. Hodgkinson, Q. h. Wu, and J. Hazel, “Empirical equations for the principal refractive indices and column angle of obliquely deposited films of tantalum oxide, titanium oxide, and zirconium oxide,” *Appl. Opt.* **37**, 2653–2659 (1998).

- [28] F. Chiadini and A. Lakhtakia, “Gaussian model for refractive indexes of columnar thin films and Bragg multilayers,” *Opt. Commun.* **231**, 257–261 (2004).
- [29] F. Chiadini and A. Lakhtakia, “Extension of Hodgkinson’s model for optical characterization of columnar thin films,” *Microw. Opt. Technol. Lett.* **42**, 72–73 (2004).
- [30] H. C. Chen, *Theory of Electromagnetic Waves: A Coordinate-Free Approach* (McGraw–Hill, 1983).
- [31] H. Hochstadt, *Differential Equations: A Modern Approach* (Dover Press, 1975).